

## Article

# Dosimetric Evaluation of $^{177}\text{Lu}$ Peptide Receptor Radionuclide Therapy Using GATE and Planet Dose

Ioanna Stamouli <sup>1</sup>, Thomas Nanos <sup>1</sup>, Konstantinos Chatzipapas <sup>2</sup>, Panagiotis Papadimitroulas <sup>3</sup>,  
Lydia-Aggeliki Zoglopitou <sup>4</sup>, Theodoros Kalathas <sup>4</sup>, Paraskevi F. Katsakiori <sup>1</sup>, Anna Makridou <sup>5</sup>  
and George C. Kagadis <sup>1,\*</sup>

- <sup>1</sup> 3dmi Research Group, Department of Medical Physics, School of Medicine, University of Patras, 26504 Rion, Greece; ioan.stamouli@gmail.com (I.S.); nanos@upatras.gr (T.N.); vkatsak@med.upatras.gr (P.F.K.)
- <sup>2</sup> Laboratoire de Traitement de l'Information Médicale (LaTIM), UMR1101, INSERM, Université de Bretagne Occidentale, 29200 Brest, France; konstantinos.chatzipapas@univ-brest.fr
- <sup>3</sup> Bioemission Technology Solutions (BIOEMTECH), 11472 Athens, Greece; panpap@bioemtech.com
- <sup>4</sup> Nuclear Medicine Department, Cancer Hospital of Thessaloniki "Theagenio", 54007 Thessaloniki, Greece; lzoglopi@gmail.com (L.-A.Z.); kalathas@dr.com (T.K.)
- <sup>5</sup> Medical Physics Department, Cancer Hospital Thessaloniki "Theagenio", 54007 Thessaloniki, Greece; anna.makridou@gmail.com
- \* Correspondence: gkagad@gmail.com

**Abstract:** This study aimed to compare the commercial dosimetric software Planet<sup>®</sup> Dose (version 3.1.1) from DOSIsoft and the open-source toolkit GATE. Dosimetry was performed for six patients receiving 200 mCi of Lutathera<sup>®</sup> every 8 weeks for four treatment cycles. For the dose calculation with Planet<sup>®</sup>, SPECT/CT images were acquired at 4, 24, 72 and 192 h post-injection. After the registration of all the time points to T<sub>0</sub>, the organs of interest (OOIs) were segmented. Time-activity curves were produced and the absorbed dose was calculated using the bi- and tri-exponential fitting methods. Regarding GATE simulations, the SPECT images of the 24 h time point were utilized for the radiopharmaceutical biodistribution in the OOIs and the attenuation maps were produced using the CT images. For liver and spleen, the average relative difference between GATE and Planet<sup>®</sup> was 9.6% and 11.1% for biexponential and 12.4% and 30.5% for triexponential fitting, respectively. The right and left kidneys showed differences up to 10.7% and 10.4% for the biexponential and up to 60.6% and 11.9% for the triexponential model, respectively. The absorbed dose calculated with GATE, Planet<sup>®</sup> (bi-exp) and Planet<sup>®</sup> (tri-exp) was in agreement with the literature. The results of the bi-exponential fitting were similar to the GATE-resulted calculations, while the tri-exponential fitting had a higher relative difference.

**Keywords:** Monte Carlo simulation; GATE; patient-specific dosimetry; peptide receptor radionuclide therapy; [ $^{177}\text{Lu}$ -[DOTA0, Tyr3]-octreotate



**Citation:** Stamouli, I.; Nanos, T.; Chatzipapas, K.; Papadimitroulas, P.; Zoglopitou, L.-A.; Kalathas, T.; Katsakiori, P.F.; Makridou, A.; Kagadis, G.C. Dosimetric Evaluation of  $^{177}\text{Lu}$  Peptide Receptor Radionuclide Therapy Using GATE and Planet Dose. *Appl. Sci.* **2023**, *13*, 9836. <https://doi.org/10.3390/app13179836>

Academic Editors: Herbert Schneckeburger and Chang Ming Charlie Ma

Received: 31 July 2023

Revised: 21 August 2023

Accepted: 29 August 2023

Published: 30 August 2023



**Copyright:** © 2023 by the authors. Licensee MDPI, Basel, Switzerland. This article is an open access article distributed under the terms and conditions of the Creative Commons Attribution (CC BY) license (<https://creativecommons.org/licenses/by/4.0/>).

## 1. Introduction

Neuroendocrine tumors (NETs) are a heterogeneous group of malignant neoplasms originating from the diffuse neuroendocrine system. NETs are not a common type of cancer, as they constitute only about 0.5% of new diagnoses [1]. These tumors can be characterized by a slow growth rate and their ability to produce and release different peptide hormones and biogenic amines [2,3]. NETs often originate in the gastroenteropancreatic tract, and among all NET types, GEP NETs are the most prevalent, accounting for 55–70% of all cases [4], while 25% start in the lung, thymus, stomach or proximal duodenum. NETs in the distal colon or rectum account for about 15% of all NETs [5].

Peptide receptor radionuclide therapy (PRRT) is a treatment that uses a radioactive isotope emitting  $\beta$  radiation, attached to a peptide delivering a high radiation dose to the tumor cells [6]. PRRT aims to target specific cell receptors, such as the somatostatin receptor

subtype 2, which is found in high levels on the surface of NETs. The most recent isotope employed for PRRT is  $^{177}\text{Lu}$ , which uses DOTA linker to form  $^{177}\text{Lu-DOTA-Tyr}^3\text{-octroate}$  ( $^{177}\text{Lu-DOTATATE}$ ) and  $^{177}\text{Lu-DOTA}^0\text{-Tyr}^3\text{-octreotide}$  ( $^{177}\text{Lu-DOTATOC}$ ) [6,7].

In recent years, there has been a significant increase in the use of computer science within the field of medical physics, particularly in the realm of personalized medicine. One of the most popular methods is the use of Monte Carlo (MC) simulations for dosimetry in both diagnostic and therapeutic applications [8,9]. Numerous studies have utilized MC simulations to calculate the absorbed doses for patients undergoing therapy with  $^{177}\text{Lu}$  [10–16]. MC simulations offer high-accuracy patient-specific dose calculations and are considered as the gold standard [17–19]. Villoing et al. aimed to validate absorbed dose calculations with the GATE MC simulation toolkit at the clinical scale for nuclear medicine dosimetry [20]. Their findings indicate that GATE provides a reliable approach for radiopharmaceutical voxel-based dosimetry [20]. However, there are practical limitations currently preventing its widespread use in daily clinical routine [21]. The main problem is that direct MC simulations are very time-consuming. Even with the technological advancements, they still need a significant amount of time, making analytical and faster alternatives more appealing [22].

Dosimetry in nuclear medicine departments has historically been a daunting task, as no commercial software was available to carry out integrated dosimetry. Advancements in dosimetry led to the development of commercial software packages, which may be used in clinical routine [23]. Mora-Ramirez et al. conducted a comparative analysis of commercial dosimetric software platforms and highlighted the necessity for the advancement of tools and standards to facilitate the comparison among such platforms. To calculate the absorbed dose, it is necessary to choose the proper fitting model for the time-activity curves [24]. Various studies suggest different fitting methods for estimating absorbed doses [25–28]. In their research, Santoro et al. conducted a comparison between Planet<sup>®</sup> Dose, Dosimetry Toolkit<sup>®</sup>, and OLINDA/EXM<sup>®</sup> V1.0, utilizing mono-exponential fitting for their analyses [29]. Similarly, Huizing et al. compared the same software packages using both mono-exponential and bi-exponential fittings [30]. Jackson et al., proposed a tri-exponential algorithm for absorbed dose calculation in patients undergoing PRRT with  $^{177}\text{Lu-DOTATATE}$  [31]. From those studies, it is evident that further research on the fitting methods is deemed necessary.

The present study aims to perform a comparative evaluation between the commercial dosimetric software Planet<sup>®</sup> Dose (DOSIsoft SA, Cachan, France) and GATE, a well-validated and reliable open-source MC simulation toolkit. Planet<sup>®</sup> Dose offers time-integrated activity coefficient (TIAC) calculation with a wide choice of interpolation methods. By comparing these two tools, our goal is to identify the optimal interpolation method and assess the accuracy and reliability of Planet<sup>®</sup> Dose. The identification of the best interpolation method through this comparison contributes to enhancing the accuracy of absorbed dose calculations and ultimately improves personalized dosimetry in clinical practice. As a result, this study would aid healthcare professionals to make more informed decisions and improve patient outcomes.

## 2. Materials and Methods

### 2.1. Patient Cohort

The dataset consists of six patients comprising five males and one female, with ages ranging from 47 to 80 years and a median age of 63, from the “Theagenio” Cancer Hospital in Thessaloniki, Greece. All patients were diagnosed with NETs and the selected treatment was PRRT with Lutathera<sup>®</sup>. Each patient received four treatment cycles, with an interval of 8 weeks between therapy cycles. The patients were administered 7400 MBq of  $^{177}\text{Lu-DOTATATE}$  with an activity concentration of 370 MBq/mL. An amino acid solution with lysine and arginine was administered to ensure renal protection. The infusion started 30 min before the Lutathera<sup>®</sup> administration and was consequently maintained for 4 h at a constant rate. Dosimetry was performed for the right and left kidneys, liver and spleen.

Intra-tumor dosimetry was not considered in the present study as the tumors' size was quite small and additional image processing was required to calculate high-resolution dose maps. Patients 1 and 6 had undergone splenectomy before receiving PRRT.

## 2.2. Image Acquisition

Four SPECT/CT images were acquired with AnyScan<sup>®</sup> SC (Mediso) for every cycle at 4 h, 24 h, 72 h and 192 h post-injection. AnyScan<sup>®</sup> SC includes a 9.5 mm NaI(Tl) crystal and nuclear medicine images were acquired using a medium-energy general purpose collimator. Energy windows of 20% centered on the 208 keV and 113 keV photopeaks were applied. Moreover, a body contour option was used for 60 projections with a duration of 20 s each and a matrix size of 128 × 128. CT images were acquired at 120 kV, exposure ≤ 100 mAs, slice thickness 1.25 mm, total collimation width 20 mm and pitch factor 1.5.

SPECT/CT images were registered and reconstructed with the "InterView<sup>™</sup> XP" program using a MC-based iterative reconstruction algorithm. The reconstruction was non-quantitative, with 48 iterations and 4 subjects. Additionally, attenuation and scatter corrections were applied based on the CT data. The parameters/dimensions of data are shown in Table 1.

**Table 1.** Data characteristics.

Modality	Resolution	Pixel Spacing	Slice Thickness
CT	527 × 527	0.977 × 0.977 mm <sup>2</sup>	2.5 mm
SPECT	128 × 128	5.474 × 5.474 mm <sup>2</sup>	5.474 mm
Dose Map	128 × 128	5.474 × 5.474 mm <sup>2</sup>	5.474 mm

## 2.3. Planet<sup>®</sup> Dose

Planet<sup>®</sup> Dose from DOSIsoft is a CE-marked software, which allows the user to perform dosimetry. Planet<sup>®</sup> was used under license at the 'Theagenio' Cancer Hospital of Thessaloniki, Greece on a dedicated workstation. Reconstructed SPECT/CT images with attenuation and scatter corrections were imported to the Planet<sup>®</sup> database. For every treatment cycle on every patient, a new study was created. SPECT/CT images of patient 4 for therapy cycle 1 were not available. In addition, patient 3 in the first cycle had only three timepoints at 4, 72, and 192 h post-Lutathera<sup>®</sup> administration, but was included in the study. Therefore, 23 dosimetry studies were created.

The first step was to register all time points to the first time point (T0). The software offers rigid, elastic and manual registration modes. In this study, rigid registration was utilized. Registration was performed based on a selected region in the coronal plane. Our region of interest (ROI) was at the abdomen, and we aimed to minimize it while ensuring that the liver, spleen and kidneys were included in that ROI. In Figure 1, the left image illustrates the ROI in the CT at the first time point (T0). The middle image represents the ROI at the second time point, and the third image shows the final, registered images. To differentiate between the two CT images, the CT of T0 is depicted with green and the CT of T1 with purple. When the two images perfectly align, the overlapping areas do not exhibit these distinct colors. The process is repeated three times to register all time points (T1, T2 and T3) to T0.

Consequently, the organs of interest (OOIs) were segmented, as seen in Figure 2, for patient 5. The segmentation in T0 was performed manually, slice by slice on the axial plane of the CT image by an expert radiologist. Hounsfield unit (HU) thresholds were applied for the liver and kidneys. For the latter, the HUs ranged from −20 to 150, while for the liver, from 0 to 150. Then, the contours were propagated to the next time points. Accurate propagation depends on successful registration, which may not always be achievable due to internal movements of the abdominal organs. As a result, manual corrections were made when it was necessary for T1, T2 and T3. The liver, the spleen and the right and left kidneys were segmented.



**Figure 1.** Registration of two CT images. Selected region of interest (Left, middle). Final result (Right). The box is used to depict the same area on both CT images and produce the correct fused image, as seen on the third part of the figure.

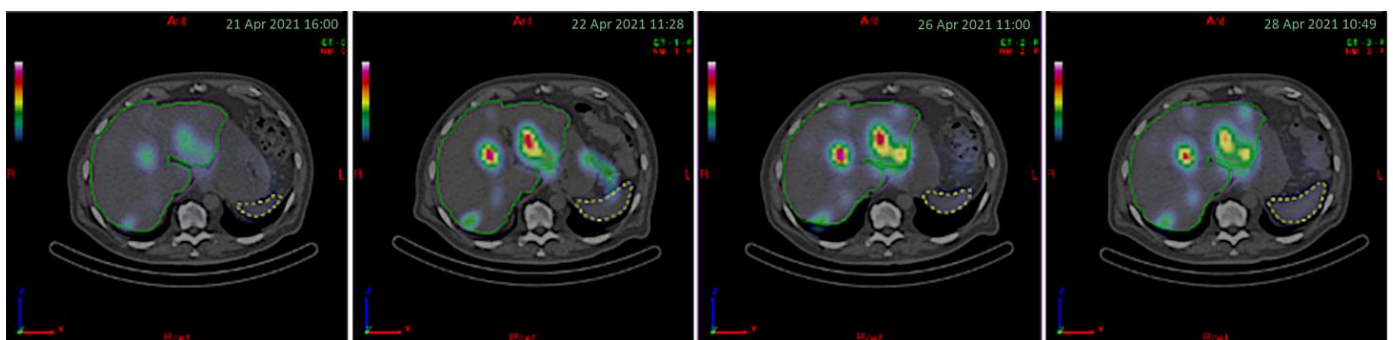


**Figure 2.** Segmented liver and spleen of patient 5 in axial slices of 4 timepoints.

A calibration factor (CF) was needed for the quantification of the SPECT/CT images. The calibration factor of the system was calculated in Bq/count depending on time per frame. SPECT images were taken with either 10 or 20 s per frame. The calibration factors were 86 and 43 Bq/count, respectively, for the two acquisition times. The injected activity for all patients was set to 7400 MBq. Time-activity curves (TACs) were generated for all segmented structures, using the Planet<sup>®</sup> software, as shown in Figure 3. Time-integrated activity coefficients (TIACs) in hours and time-integrated activity (TIA) in MBq·sec were calculated with the interpolation method, as implemented in Planet<sup>®</sup>. S-values were calculated via the convolution of the absorbed dose voxel kernel (dose kernels) with density correction. Finally, the mean absorbed dose was calculated using the area under the curve (AUC), as specified by the fitting model. In this study, both bi- and tri-exponential fittings were applied. The bi-exponential model is described by:

$$y = a_1e^{b_1t} + a_2e^{b_2t} \tag{1}$$

And the tri-exponential by:

$$y = a_3e^{b_3t} + a_4e^{b_4t} + a_5e^{b_5t} \tag{2}$$

where  $y$  is the average absorbed dose rate ( $\mu\text{Gy}/\text{sec}$ ),  $t$  is the time (h) and  $a_1, a_2, a_3, a_4, a_5, b_1, b_2, b_3, b_4, b_5$  are constant values.

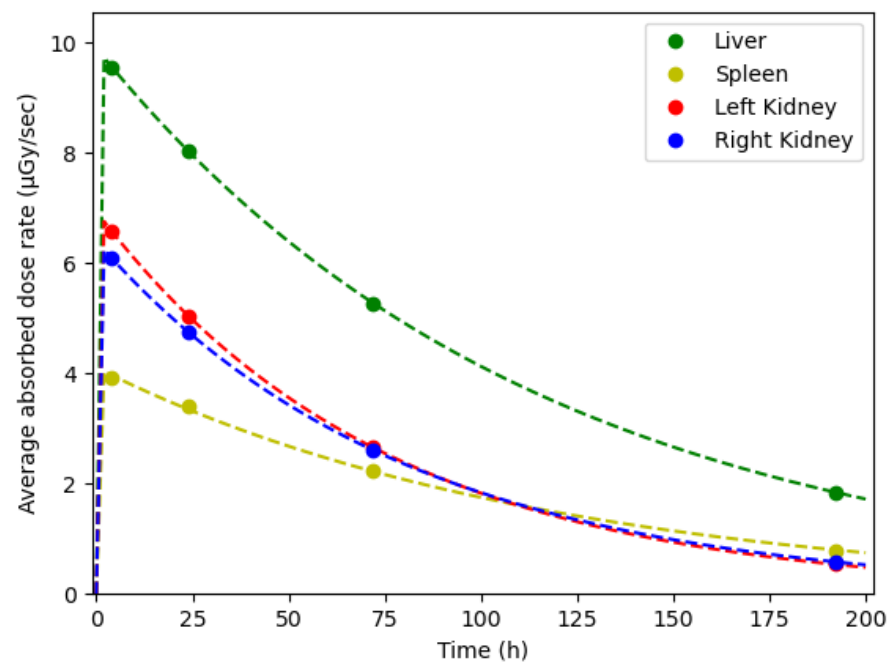


**Figure 3.** TACs for the liver (green), the spleen (yellow), the right (blue) and left (red) kidney of patient 5.

#### 2.4. Pre-Processing

Contours from PLANET<sup>®</sup> were exported as RT-Structure files to be used for MC simulations. GATE requires all imported data to be oriented as RAI (Right Anterior Inferior) and have the same dimensions. 3D-Slicer v.5.0.3 was employed to convert the contours to label map volumes and then for orientation and resizing [32]. The ‘Orient Scalar Volume’ module was used for the orientation. Then, for the resizing, we utilized the ‘Resample Scalar Volume’ module, which implements image resampling via itk Transforms. All images were transformed to  $128 \times 128 \times 128$  size. The resampling parameters are the spacing and the interpolation. The new element spacing was calculated by:

$$s_i' = \frac{d_i}{128} \cdot s_i, i = x, y, z \quad (3)$$

where  $d_i$  is the original size and  $s_i$  is the original element spacing of the  $i$ -dimension. Linear interpolation was used for the CT and SPECT images, while the nearest neighbor interpolation method was used for label maps. The new images were saved as header files (.mhd).

#### 2.5. GATE Toolkit

The GATE v9.1 MC simulations toolkit was used in the present study to produce dosimetric data [33,34]. We used GATE to simulate the dosimetry corresponding to the biodistribution of a single time point. Dose actors were used to calculate the absorbed dose in voxel-by-voxel level (dose map). Following radiopharmaceutical administration, there is an initial phase of uptake. Subsequently, once the uptake reaches its maximum level, a washout phase occurs. The duration of the washout is determined by the physical and biological half-life of the radiopharmaceutical. The 24 h time point was chosen for the simulations due to the high concentration of the radiopharmaceutical in the OOI. Consequently, the SPECT/CT images and the contours of the 24 h time point (T1) were used. The only exception was the first cycle of patient 3, where only the 4 h, 72 h and 192 h time points were available and T0 was chosen instead. The SPECT images and the <sup>177</sup>Lu spectrum defined the source (activity map inserted in GATE), while the activity was set to 7400 MBq. Regarding the <sup>177</sup>Lu spectrum, it was defined through a histogram spectrum,

originating from a point source. The energy distribution was set using the arbitrary point-wise method of GATE (Arb). The minimum energy was set to 0 MeV and the maximum to 0.498 MeV. This range was selected based on the  $^{177}\text{Lu}$  emission spectrum [35,36]. The source was placed at coordinates (0,0,0) on the x, y and z axes. The angular distribution of the emission of the source was isotropic. The theta angle was set from 0 to 180 degrees, while the phi angle ranged from 0 to 360 degrees.

The CT images were employed to generate materials from HUs and define the attenuation computational phantom using the ‘ImageNestedParametrisedVolume’ method. The emstandard\_opt4 physics constructor were used to simulate the interactions of radiation with matter. Emstandard\_opt4 provides high accuracy electron, hadron and ion tracking, incorporating the most accurate standard and low energy models for electromagnetic physical processes [37–39]. The ‘DoseActor’ was utilized for dose calculation, and was attached to the CT phantom with ‘Edep’ and ‘UncertaintyEdep’ enabled. This allowed the storage of deposited energy and the statistical uncertainty in the 3D dose map. The ‘SimulationStatisticActor’ was used to record the number of events during the simulation. The Mersenne Twister generator was employed as the random generator. Each simulation was executed or  $2 \times 10^9$  primaries, to achieve a high level of accuracy, resulting also to a low level of statistical uncertainty, which was calculated  $\leq 2\%$  for every organ of interest (OOI). In-house Python scripts were utilized to obtain the final results, regarding the estimation of Dose per OOI. Based on our clinical experience and the available literature, we defined the liver, spleen, right kidney and left kidney as organs of interest [40,41].

### 3. Results

For every patient, the absorbed dose was calculated for the liver, spleen, left and right kidney with three methods using Planet<sup>®</sup> Dose with bi- and tri-exponential fitting, and the Gate Toolkit. Box-plots, as shown in Figure 4, were constructed for the absorbed dose calculated with every method for the OOIs. Table 2 presents the percentage differences between the calculation methods as calculated by:

$$RD = \frac{|experimental\ value - reference\ value|}{reference\ value} \cdot 100\% \quad (4)$$

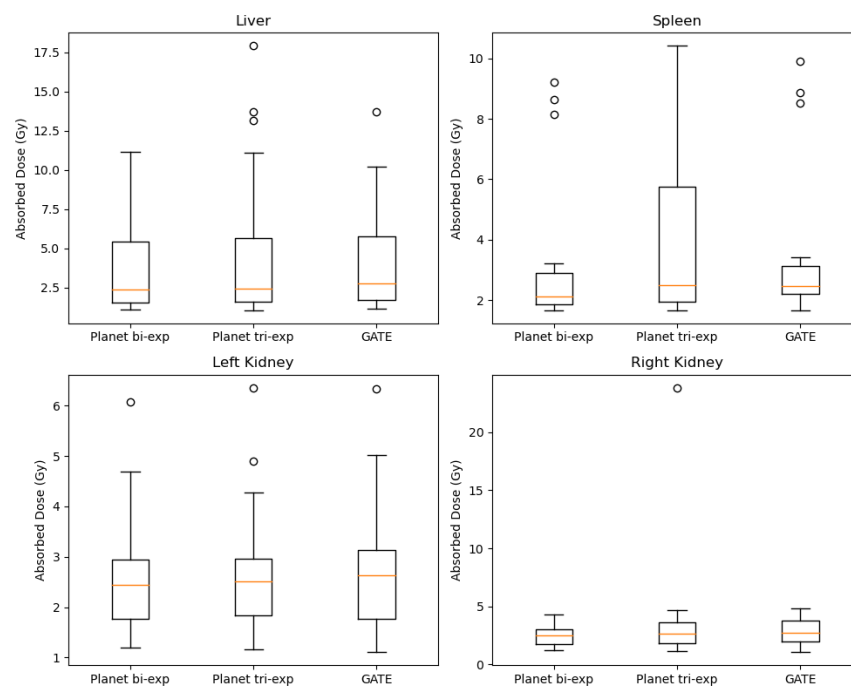


**Figure 4.** Average absorbed dose calculated for liver, spleen and right and left kidney.

**Table 2.** Differences between the calculation methods.

Patient No.	Cycle No.	Liver (Difference %)			Spleen (Difference %)			Right Kidney (Difference %)			Left Kidney (Difference %)			Average Difference (%)		
		Bi vs. Tri	Bi vs. Gate	Tri vs. Gate	Bi vs. Tri	Bi vs. Gate	Tri vs. Gate	Bi vs. Tri	Bi vs. Gate	Tri vs. Gate	Bi vs. Tri	Bi vs. Gate	Tri vs. Gate	Bi vs. Tri	Bi vs. Gate	Tri vs. Gate
1	1	3.3	18.0	15.3				88.4	17.5	121.3	0.0	17.7	17.7	8.53	14.27	21.93
	2	4.5	15.2	11.5				0.3	25.6	25.3	0.0	2.3	2.3			
	3	1.5	13.7	12.3				0.0	16.4	16.4	0.1	6.2	6.3			
	4	4.2	8.0	4.1				0.0	17.6	17.6	0.0	13.0	13.0			
2	1	14.4	0.9	15.5	0.0	32.1	32.1	39.0	32.5	6.2	33.6	12.5	50.3	35.42	15.21	37.36
	2	0.0	5.8	5.8	444.1	17.5	348.9	3.3	10.3	7.4	0.0	23.0	23.0			
	3	3.9	2.3	6.1	0.0	0.2	0.2	1.4	11.9	10.3	2.7	32.2	34.0			
	4	16.0	18.9	5.9	6.3	4.1	10.6	2.1	15.7	18.1	0.1	23.4	23.4			
3	1	22.9	18.4	0.3	14.2	31.1	21.3	1218.5	9.3	1095.5	0.1	15.8	15.7	88.11	11.35	83.79
	2	27.8	11.3	42.3	23.4	15.8	3.9	0.2	9.5	9.4	6.3	12.9	20.0			
	3	3.8	18.6	23.1	2.7	10.1	7.7	5.2	9.2	4.4	1.1	3.6	4.8			
	4	80.1	2.4	75.7	0.3	5.9	5.6	0.0	1.4	1.4	3.2	6.4	9.8			
4	1							N/A						2.19	5.80	4.03
	2	3.6	3.8	0.4	3.9	7.1	3.5	4.3	9.3	5.4	2.3	3.5	1.3			
	3	6.1	4.3	1.5	3.1	2.7	0.3	0.1	6.2	6.1	0.0	8.9	8.9			
	4	1.1	5.6	4.6	1.8	4.4	2.6	0.0	5.8	5.8	0.0	8.0	8.0			
5	1	6.7	4.1	2.3	11.7	11.5	1.1	0.1	6.2	6.1	2.9	5.8	3.1	5.35	7.59	5.64
	2	17.2	4.9	11.4	6.9	13.5	7.6	6.1	10.1	4.6	16.6	10.1	4.8			
	3	0.0	11.6	11.6	1.3	7.4	8.6	0.9	4.0	4.8	0.0	6.1	6.1			
	4	7.9	9.8	2.8	7.4	4.0	3.1	0.0	7.4	7.3	0.0	4.9	4.9			
6	1	5.8	12.0	6.9				3.5	11.6	8.5	4.4	4.0	0.2	2.04	7.22	5.68
	2	0.0	7.4	7.4				1.6	3.9	5.6	4.2	6.4	2.5			
	3	0.0	8.5	8.5				0.0	1.3	1.3	0.0	7.0	7.0			
	4	4.8	14.2	10.0				0.1	4.4	4.3	0.0	5.9	5.9			

In the comparison between GATE and Planet<sup>®</sup>, the absorbed doses from GATE were considered reference values and those calculated with Planet<sup>®</sup> were the experimental values. In the comparison between the biexponential and triexponential fitting, the biexponential was considered as reference.

The average relative differences between GATE and Planet<sup>®</sup> for every organ are presented in Table 3.

**Table 3.** Average relative difference (%) between Planet<sup>®</sup> methods and GATE.

Organ	Average Relative Difference (%)	
	GATE vs. Planet <sup>®</sup> (bi-exp)	GATE vs. Planet <sup>®</sup> (tri-exp)
Liver	9.6	12.4
Spleen	11.1	30.5
Right Kidney	10.7	60.6
Left Kidney	10.4	11.9

Bland–Altman plots, as shown in Figure 5, were also constructed for every organ of interest to visualize the absorbed dose differences between Planet<sup>®</sup> (bi-exp) and GATE. The red and blue lines indicate the means of the differences between GATE and the biexponential fitting and triexponential fitting, respectively. The dotted lines represent the 95% confidence intervals (CIs) of the differences.

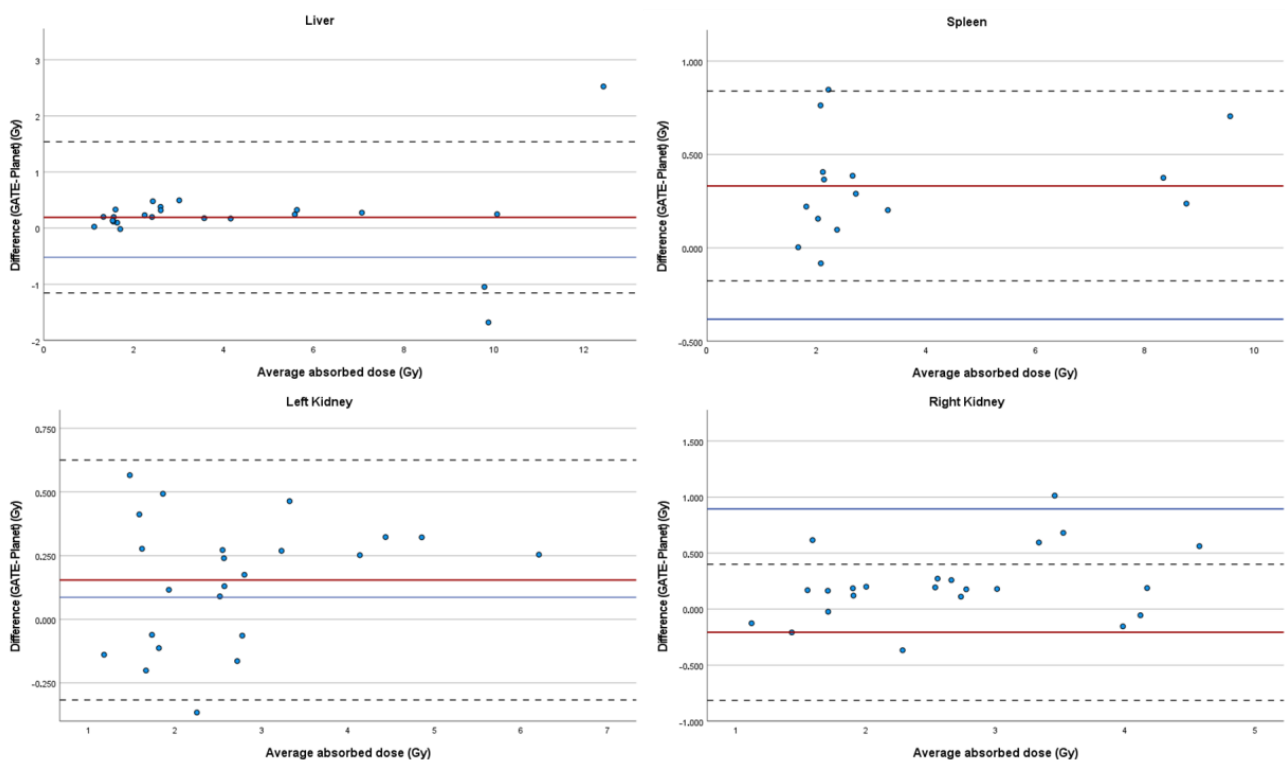


**Figure 5.** Bland–Altman plots for every organ.

Stacked bar charts of the absorbed dose by patient are presented in Figure 6. The absorbed dose values are those computed by GATE, which are considered our reference values.

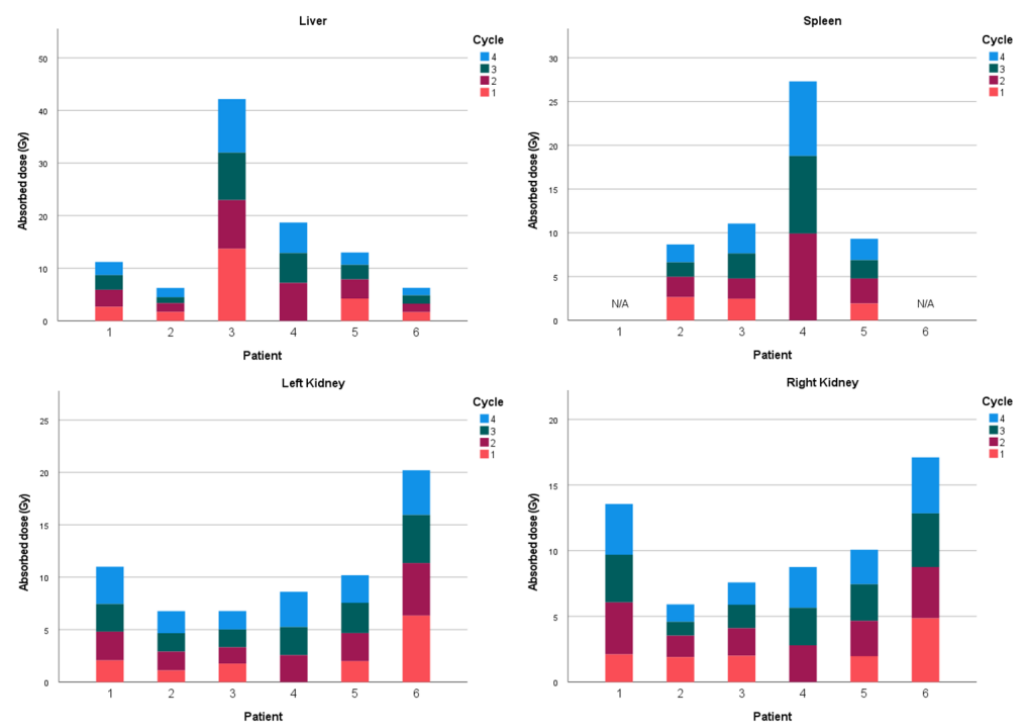


**Figure 6.** Cumulative absorbed dose per patient for liver, spleen and right and left kidney.

#### 4. Discussion

The purpose of this study was the dosimetric evaluation of Lutathera<sup>®</sup>. For the dose calculation, we used GATE for MC simulations and the Planet<sup>®</sup> Dose software from DOSIsoft. The mean absorbed doses for every organ agree with the available literature [16,29,41,42].

Regarding the comparison between GATE and Planet<sup>®</sup>, we observe that the bi-exponential fitting of the TACs presented similar results with GATE. The average relative difference between them is less than 11.1% for every organ (Table 3). The differences can be explained by our limited sample size ( $n = 15$  for spleen and  $n = 23$  for liver and kidneys), the method that the CF was calculated, as well as the difference in the technique of both methods. Planet<sup>®</sup> makes an estimation of dose while considering the TACs, in comparison to GATE, where only one specific time point was considered. Nevertheless, both techniques are an estimation procedure that has a lot of room for improvement.

An error-prone experimental set up may introduce uncertainties and affect dose calculation. The Bland–Altman plots demonstrate that there is no proportional bias between GATE and Planet<sup>®</sup> (bi-exp), and the mean of the differences is close to zero for all organs. Moreover, we observed that most of the differences (GATE–Planet<sup>®</sup> (bi-exp)) are positive for all organs. This may indicate that the CF has a slightly higher value than the defined. However, the limits of agreement were less than 1 Gy for the spleen and the left and right kidneys, and slightly higher for the liver. On the other hand, the results of the tri-exponential fitting are not satisfactory. The tri-exponential fitting considers an uptake phase, a rapid and a long-term clearance phase, which accurately describes the pharmacokinetics. Despite that, the relative differences between GATE and Planet<sup>®</sup> (tri-exp) are 60.6% and 30.5% for right kidney and spleen, respectively. This indicates that four time points are not enough for tri-exponential fitting. Furthermore, there is a calculated value of absorbed doses that shows a large difference to the mean value, which may be attributed to the small dataset.

Based on prior knowledge regarding renal absorbed dose tolerance from external beam radiation therapy, the dose limit for kidneys is 23 Gy. In addition, the biologically effective dose (BED) for PRRT with <sup>177</sup>Lu has been estimated to be 40 Gy for patients without risk factors for renal toxicity and 28 Gy for those with risk factors [43]. Figure 6 shows that

none of these limits were exceeded. However, we observed that the cumulative absorbed dose indicates significant intra-patients' variations, even though the administered activity was the same. The aforementioned variations pose the need for patient-specific dosimetry calculation in nuclear medicine therapeutic applications.

The main limitations of the present study are the small data sample and the lack of dose calculation within lesions. Further studies should be conducted in the future, comparing GATE and Planet<sup>®</sup> Dose (bi-exp), to obtain more robust results.

## 5. Conclusions

The main objective of this study was to perform a dosimetric evaluation of Lutathera<sup>®</sup> and compare the results between GATE and Planet<sup>®</sup> Dose. The findings show that the absorbed doses calculated using either MC simulations with GATE or the commercially available Planet<sup>®</sup> Dose software are acceptable. Regarding Planet<sup>®</sup>, the bi-exponential fitting of the TACs is superior to the tri-exponential fitting when four time points are used.

Overall, both toolkits can be used for the dosimetry of PRRT with Lutathera<sup>®</sup>, as they provide optimal and patient-specific results.

**Author Contributions:** Data curation, L.-A.Z., T.K. and P.F.K.; Dose calculation, K.C., P.P., G.C.K. and I.S.; CT scan evaluation and interpretation, T.K., P.F.K. and G.C.K.; Formal analysis, K.C., P.F.K., A.M., P.P. and G.C.K.; Funding acquisition, G.C.K.; Investigation, I.S., T.N., K.C., L.-A.Z., P.F.K., A.M., P.P. and G.C.K.; Methodology, I.S., T.N., K.C., P.F.K., A.M., P.P. and G.C.K.; Project administration, G.C.K.; Resources, I.S., L.-A.Z., T.K., A.M. and G.C.K.; Software, T.N. and P.P.; Supervision, P.P. and G.C.K.; Validation, I.S., K.C., P.P. and G.C.K.; Visualization, I.S. and P.F.K.; Writing—original draft, I.S., K.C., P.F.K. and A.M.; Writing—review and editing, P.P. and G.C.K. All authors have read and agreed to the published version of the manuscript.

**Funding:** This research is co-financed by: (a) European Union's Horizon 2020 research and innovation program under the Marie Skłodowska-Curie grant agreement No 872735. The results published in this study reflect only the author's view and the Research Executive Agency (REA) and the European Commission is not responsible for any use that may be made of the information it contains, (b) the European Regional Development Fund (ERDF), Greek General Secretariat for Research and Innovation, Operational Programme "Competitiveness, Entrepreneurship and Innovation" (EPAnEK), under the frame of ERA PerMed (project POPEYE T11EPA4-00055), and (c) the Hellenic Foundation for Research and Innovation (H.F.R.I.) under the "2nd call for H.F.R.I. research projects to support faculty members & researchers" (project number: 2692).

**Institutional Review Board Statement:** The study was conducted in accordance with the Declaration of Helsinki, and approved by the Institutional Review Board of Cancer Hospital of Thessaloniki "Theagenio" (17201/31-10-2022).

**Informed Consent Statement:** Informed consent was obtained from all subjects involved in the study.

**Data Availability Statement:** The data presented in this study are available on request from the corresponding author. The data are not publicly available due to ethical restrictions.

**Conflicts of Interest:** The authors declare no conflict of interest.

## References

1. Oronsky, B.; Ma, P.C.; Morgensztern, D.; Carter, C.A. Nothing But NET: A Review of Neuroendocrine Tumors and Carcinomas. *Neoplasia* **2017**, *19*, 991–1002. [[CrossRef](#)] [[PubMed](#)]
2. PDQ Adult Treatment Editorial Board. Gastrointestinal Neuroendocrine Tumors Treatment (PDQ<sup>®</sup>): Health Professional Version. 2002. Available online: <https://www.ncbi.nlm.nih.gov/books/NBK65769/> (accessed on 30 July 2023).
3. Cives, M.; Strosberg, J.R. Gastroenteropancreatic Neuroendocrine Tumors. *CA A Cancer J. Clin.* **2018**, *68*, 471–487. [[CrossRef](#)]
4. Das, S.; Dasari, A. Epidemiology, Incidence, and Prevalence of Neuroendocrine Neoplasms: Are There Global Differences? *Curr. Oncol. Rep.* **2021**, *23*, 43. [[CrossRef](#)]
5. Panagiotidis, E.; Bomanji, J. Role of 18F-Fluorodeoxyglucose PET in the Study of Neuroendocrine Tumors. *PET Clin.* **2014**, *9*, 43–55. [[CrossRef](#)] [[PubMed](#)]

6. Zaknun, J.J.; Bodei, L.; Mueller-Brand, J.; Pavel, M.E.; Baum, R.P.; Hörsch, D.; O'Doriso, M.S.; O'Dorisiol, T.M.; Howe, J.R.; Cremonesi, M.; et al. The joint IAEA, EANM, and SNMMI practical guidance on peptide receptor radionuclide therapy (PRRT) in neuroendocrine tumours. *Eur. J. Nucl. Med. Mol. Imaging* **2013**, *40*, 800–816. [[CrossRef](#)]
7. Dash, A.; Chakraborty, S.; Pillai, M.R.A.; Knapp, F.F. Peptide Receptor Radionuclide Therapy: An Overview. *Cancer Biother. Radiopharm.* **2015**, *30*, 47–71. [[CrossRef](#)] [[PubMed](#)]
8. Papadimitroulas, P. Dosimetry applications in GATE Monte Carlo toolkit. *Phys. Medica* **2017**, *41*, 136–140. [[CrossRef](#)]
9. Chatzipapas, K.P.; Papadimitroulas, P.; Emfietzoglou, D.; Kalospyros, S.A.; Hada, M.; Georgakilas, A.G.; Kagadis, G.C. Ionizing Radiation and Complex DNA Damage: Quantifying the Radiobiological Damage Using Monte Carlo Simulations. *Cancers* **2020**, *12*, 799. [[CrossRef](#)]
10. Eleftheriadis, V.; Savvidis, G.; Paneta, V.; Chatzipapas, K.; Kagadis, G.C.; Papadimitroulas, P. A framework for prediction of personalized pediatric nuclear medical dosimetry based on machine learning and Monte Carlo techniques. *Phys. Med. Biol.* **2023**, *68*, 084004. [[CrossRef](#)]
11. Hippeläinen, E.; Tenhunen, M.; Sohlberg, A. Fast voxel-level dosimetry for  $^{177}\text{Lu}$  labelled peptide treatments. *Phys. Med. Biol.* **2015**, *60*, 6685–6700. [[CrossRef](#)]
12. Kost, S.D.; Dewaraja, Y.K.; Abramson, R.G.; Stabin, M.G. VIDA: A Voxel-Based Dosimetry Method for Targeted Radionuclide Therapy Using Geant4. *Cancer Biother. Radiopharm.* **2015**, *30*, 16–26. [[CrossRef](#)]
13. Lee, M.S.; Hwang, D.; Kim, J.H.; Lee, J.S. Deep-dose: A voxel dose estimation method using deep convolutional neural network for personalized internal dosimetry. *Sci. Rep.* **2019**, *9*, 10308. [[CrossRef](#)]
14. Ligonnet, T.; Pistone, D.; Auditore, L.; Italiano, A.; Amato, E.; Campenni, A.; Schaefer, N.; Boughdad, S.; Baldari, S.; Gnesin, S. Simplified patient-specific renal dosimetry in  $^{177}\text{Lu}$  therapy: A proof of concept. *Phys. Medica* **2021**, *92*, 75–85. [[CrossRef](#)]
15. Gosewisch, A.; Ilhan, H.; Tattenberg, S.; Mairani, A.; Parodi, K.; Brosch, J.; Kaiser, L.; Gildehaus, F.J.; Todica, A.; Ziegler, S.; et al. 3D Monte Carlo bone marrow dosimetry for Lu-177-PSMA therapy with guidance of non-invasive 3D localization of active bone marrow via Tc-99m-anti-granulocyte antibody SPECT/CT. *EJNMMI Res.* **2019**, *9*, 76. [[CrossRef](#)]
16. Goetz, T.I.; Lang, E.W.; Prante, O.; Maier, A.; Cordes, M.; Kuwert, T.; Ritt, P.; Schmidkonz, C. Three-dimensional Monte Carlo-based voxel-wise tumor dosimetry in patients with neuroendocrine tumors who underwent  $^{177}\text{Lu}$ -DOTATOC therapy. *Ann. Nucl. Med.* **2020**, *34*, 244–253. [[CrossRef](#)]
17. Papadimitroulas, P.; Erwin, W.D.; Iliadou, V.; Kostou, T.; Loudos, G.; Kagadis, G.C. A personalized, Monte Carlo-based method for internal dosimetric evaluation of radiopharmaceuticals in children. *Med. Phys.* **2018**, *45*, 3939–3949. [[CrossRef](#)]
18. Papadimitroulas, P.; Kostou, T.; Chatzipapas, K.; Visvikis, D.; Mountris, K.A.; Jaouen, V.; Katsanos, K.; Diamantopoulos, A.; Apostolopoulos, D.; Balomenos, A.; et al. A Review on Personalized Pediatric Dosimetry Applications Using Advanced Computational Tools. *IEEE Trans. Radiat. Plasma Med. Sci.* **2019**, *3*, 607–620. [[CrossRef](#)]
19. Alsadi, R.; Djekidel, M.; Bouhali, O.; Doherty, J.O. Towards Routine Clinical Use of Dosimetry in [ $^{177}\text{Lu}$ ]Lu-PSMA Prostate Cancer Radionuclide Therapy: Current Efforts and Future Perspectives. *Front. Phys.* **2022**, *10*, 618. [[CrossRef](#)]
20. Villoing, D.; Marcatili, S.; Garcia, M.-P.; Bardiès, M. Internal dosimetry with the Monte Carlo code GATE: Validation using the ICRP/ICRU female reference computational model. *Phys. Med. Biol.* **2017**, *62*, 1885–1904. [[CrossRef](#)] [[PubMed](#)]
21. Tsougos, I.; Loudos, G.; Georgoulas, P.; Theodorou, K.; Kappas, C. Patient-specific internal radionuclide dosimetry. *Nucl. Med. Commun.* **2010**, *31*, 97–106. [[CrossRef](#)]
22. Papadimitroulas, P.; Loudos, G.; Nikiforidis, G.C.; Kagadis, G.C. A dose point kernel database using GATE Monte Carlo simulation toolkit for nuclear medicine applications: Comparison with other Monte Carlo codes. *Med. Phys.* **2012**, *39*, 5238–5247. [[CrossRef](#)] [[PubMed](#)]
23. Della Gala, G.; Bardiès, M.; Tipping, J.; Strigari, L. Overview of commercial treatment planning systems for targeted radionuclide therapy. *Phys. Medica* **2021**, *92*, 52–61. [[CrossRef](#)] [[PubMed](#)]
24. Mora-Ramirez, E.; Santoro, L.; Cassol, E.; Ocampo-Ramos, J.C.; Clayton, N.; Kayal, G.; Chouaf, S.; Trauchessec, D.; Pouget, J.; Kotzki, P.; et al. Comparison of commercial dosimetric software platforms in patients treated with  $^{177}\text{Lu}$ -DOTATATE for peptide receptor radionuclide therapy. *Med. Phys.* **2020**, *47*, 4602–4615. [[CrossRef](#)]
25. Sarrut, D.; Halty, A.; Badel, J.-N.; Ferrer, L.; Bardiès, M. Voxel-based multimodel fitting method for modeling time activity curves in SPECT images. *Med. Phys.* **2017**, *44*, 6280–6288. [[CrossRef](#)]
26. Zhao, W.; Esquinas, P.L.; Frezza, A.; Hou, X.; Beaugard, J.-M.; Celler, A. Accuracy of kidney dosimetry performed using simplified time activity curve modelling methods: A  $^{177}\text{Lu}$ -DOTATATE patient study. *Phys. Med. Biol.* **2019**, *64*, 175006. [[CrossRef](#)]
27. Rinscheid, A.; Kletting, P.; Eiber, M.; Beer, A.J.; Glatting, G. Influence of sampling schedules on [ $^{177}\text{Lu}$ ]Lu-PSMA dosimetry. *EJNMMI Phys.* **2020**, *7*, 41. [[CrossRef](#)]
28. Marin, G.; Vanderlinden, B.; Karfis, I.; Guiot, T.; Wimana, Z.; Reynaert, N.; Vandenberghe, S.; Flamen, P. A dosimetry procedure for organs-at-risk in  $^{177}\text{Lu}$  peptide receptor radionuclide therapy of patients with neuroendocrine tumours. *Phys. Medica* **2018**, *56*, 41–49. [[CrossRef](#)] [[PubMed](#)]
29. Santoro, L.; Pitalot, L.; Trauchessec, D.; Mora-Ramirez, E.; Kotzki, P.O.; Bardiès, M.; Deshayes, E. Clinical implementation of PLANET<sup>®</sup> Dose for dosimetric assessment after [ $^{177}\text{Lu}$ ]Lu-DOTA-TATE: Comparison with Dosimetry Toolkit<sup>®</sup> and OLINDA/EXM<sup>®</sup> V1.0. *EJNMMI Res.* **2021**, *11*, 1. [[CrossRef](#)]

30. Huizing, D.M.V.; Peters, S.M.B.; Versleijen, M.W.J.; Martens, E.; Verheij, M.; Sinaasappel, M.; Stokkel, M.P.M.; Veen, B.J.d.W.-V.d. A head-to-head comparison between two commercial software packages for hybrid dosimetry after peptide receptor radionuclide therapy. *EJNMMI Phys.* **2020**, *7*, 36. [[CrossRef](#)]
31. Jackson, P.; McIntosh, L.; Hofman, M.S.; Kong, G.; Hicks, R.J. Technical Note: Rapid multiexponential curve fitting algorithm for voxel-based targeted radionuclide dosimetry. *Med. Phys.* **2020**, *47*, 4332–4339. [[CrossRef](#)]
32. Fedorov, A.; Beichel, R.; Kalpathy-Cramer, J.; Finet, J.; Fillion-Robin, J.-C.; Pujol, S.; Bauer, C.; Jennings, D.; Fennessy, F.; Sonka, M.; et al. 3D Slicer as an image computing platform for the Quantitative Imaging Network. *Magn. Reson. Imaging* **2012**, *30*, 1323–1341. [[CrossRef](#)]
33. Agostinelli, S.; Allison, J.; Amako, K.; Apostolakis, J.; Araujo, H.; Arce, P.; Asai, M.; Axen, D.; Banerjee, S.; Barrand, G.; et al. Geant4—A simulation toolkit. *Nucl. Instrum. Methods Phys. Res. Sect. A* **2003**, *506*, 250–303. [[CrossRef](#)]
34. Jan, S.; Benoit, D.; Becheva, E.; Carlier, T.; Cassol, F.; Descourt, P.; Frisson, T.; Grevillot, L.; Guigues, L.; Maigne, L.; et al. GATE V6: A major enhancement of the GATE simulation platform enabling modelling of CT and radiotherapy. *Phys. Med. Biol.* **2011**, *56*, 881–901. [[CrossRef](#)]
35. European Medicines Agency. Lutathera: EPAR—Product Information. Updated 25 October 2022. Available online: <https://www.ema.europa.eu/en/medicines/human/EPAR/lutathera> (accessed on 6 July 2023).
36. Dash, A.; Pillai, M.R.A.; Knapp, F.F., Jr. Production of  $^{177}\text{Lu}$  for Targeted Radionuclide Therapy: Available Options. *Nucl. Med. Mol. Imaging* **2010**, *49*, 85–107. [[CrossRef](#)]
37. Moshkbar-Bakhshayesh, K.; Mohtashami, S. Developing an approach for fast estimation of range of ion in interaction with material using the Geant4 toolkit in combination with the neural network. *Nucl. Eng. Technol.* **2022**, *54*, 4209–4214. [[CrossRef](#)]
38. Wellisch, J.P.; Kossov, M.; Degtyarenko, P. Electro and Gamma Nuclear Physics in Geant4. June 2003. Available online: <http://arxiv.org/abs/nucl-th/0306012> (accessed on 30 July 2023).
39. Geant4 Collaboration. Physics Reference Manual. GEANT4 A Simulation Toolkit, Volume 1, pp. 1–554. 2019. Available online: <https://geant4-userdoc.web.cern.ch/UsersGuides/PhysicsReferenceManual/fo/PhysicsReferenceManual.pdf> (accessed on 30 July 2023).
40. Gleisner, K.S.; Chouin, N.; Gabina, P.M.; Cicone, F.; Gnesin, S.; Stokke, C.; Konijnenberg, M.; Cremonesi, M.; Verburg, F.A.; Bernhardt, P.; et al. EANM dosimetry committee recommendations for dosimetry of  $^{177}\text{Lu}$ -labelled somatostatin-receptor- and PSMA-targeting ligands. *Eur. J. Nucl. Med. Mol. Imaging* **2022**, *49*, 1778–1809. [[CrossRef](#)]
41. Santoro, L.; Mora-Ramirez, E.; Trauchessec, D.; Chouaf, S.; Eustache, P.; Pouget, J.-P.; Kotzki, P.-O.; Bardiès, M.; Deshayes, E. Implementation of patient dosimetry in the clinical practice after targeted radiotherapy using [ $^{177}\text{Lu}$ -[DOTA0, Tyr3]-octreotate. *EJNMMI Res.* **2018**, *8*, 103. [[CrossRef](#)]
42. Vergnaud, L.; Giraudet, A.-L.; Moreau, A.; Salvadori, J.; Imperiale, A.; Baudier, T.; Badel, J.-N.; Sarrut, D. Patient-specific dosimetry adapted to variable number of SPECT/CT time-points per cycle for  $^{177}\text{Lu}$ -DOTATATE therapy. *EJNMMI Phys.* **2022**, *9*, 37. [[CrossRef](#)]
43. Svensson, J.; Berg, G.; Wängberg, B.; Larsson, M.; Forssell-Aronsson, E.; Bernhardt, P. Renal function affects absorbed dose to the kidneys and haematological toxicity during  $^{177}\text{Lu}$ -DOTATATE treatment. *Eur. J. Nucl. Med. Mol. Imaging* **2015**, *42*, 947–955. [[CrossRef](#)]

**Disclaimer/Publisher’s Note:** The statements, opinions and data contained in all publications are solely those of the individual author(s) and contributor(s) and not of MDPI and/or the editor(s). MDPI and/or the editor(s) disclaim responsibility for any injury to people or property resulting from any ideas, methods, instructions or products referred to in the content.